BBA - General Subjects 1861 (2017) 2099–2111

Contents lists available at ScienceDirect

BBA - General Subjects

journal homepage: www.elsevier.com/locate/bbagen

Investigation of calcium-dependent activity and conformational dynamics of zebra fish 12-lipoxygenase

Monica Mittal[a,*], Mahmudul Hasan[b,c], Navisraj Balagunaseelan[a], Alexander Fauland[a], Craig Wheelock[a], Olof Rådmark[a], Jesper Z. Haeggström[a], Agnes Rinaldo-Matthis[a]

[a] Department of Medical Biochemistry and Biophysics, Division of Chemistry II, 17177 Stockholm, Sweden
[b] Department of Biochemistry and Structural Biology, Center for Molecular Protein Science, Lund University, POB 124, 22100 Lund, Sweden
[c] Crystallization Facility, Department of Biology, Lund University, Sölvegatan 35, 22362 Lund, Sweden

ARTICLE INFO

Keywords:
Eicosanoids
Lipoxygenases
Calcium
Activity
SAXS
Dynamic light scattering

ABSTRACT

Background: A 12-lipoxygenase in zebra fish (*zf*12-LOX) was found to be required for normal embryonic development and LOXs are of great interest for targeted drug designing. In this study, we investigate the structural-functional aspects of *zf*12-LOX in response to calcium.

Methods: A soluble version of *zf*12-LOX was created by mutagenesis. Based on multiple sequence alignment, we mutated the putative calcium-responsive amino acids in N-PLAT domain of soluble *zf*12-LOX. Using a series of biophysical methods, we ascertained the oligomeric state, stability, structural integrity and conformational changes of *zf*12-LOX in response to calcium. We also compared the biophysical properties of soluble *zf*12-LOX with the mutant in the absence and presence of calcium.

Results: Here we provide a detailed characterization of soluble *zf*12-LOX and the mutant. Both proteins exist as compact monomers in solution, however the enzyme activity of soluble *zf*12-LOX is significantly increased in presence of calcium. We find that the stimulatory effect of calcium on *zf*12-LOX is related to a change in protein structure as observed by SAXS, adopting an *open-state*. In contrast, enzyme with a mutated calcium regulatory site has reduced activity-response to calcium and restricted large re-modeling, suggesting that it retains a closed-state in response to calcium. Taken together, our study suggests that Ca^{2+}-dependent regulation is associated with different domain conformation(s) that might change the accessibility to substrate-binding site in response to calcium.

General significance: The study can be broadly implicated in better understanding the mode(s) of action of LOXs, and the enzymes regulated by calcium in general.

1. Introduction

Lipoxygenases (LOXs) are non-heme iron containing oxygenases, which catalyze polyunsaturated fatty acids (PUFA) into lipid-hydroperoxides. The catalysis products of arachidonic acid (AA), one of the main PUFA in animals, are hydroeicosatetraenoic (HETEs) or hydroperoxyeicosatetraenoic acids (HpETEs). These lipid mediators and their metabolites have been implicated in cancer, atherosclerosis and allergic inflammation [1–4]. Consequently, LOXs are pivotal targets for drug design [5,6]. Calcium is known to be a key regulatory factor in determining cellular physiology and studies primarily on five LOXs (mammalian 5-LOX, *Plexaura homomalla* coral 8R-LOX, *Gersemia fruticosa* coral 11R-LOX, human 15-LOX-2, and 15-LOX-1) have provided insight about Ca^{2+} binding (μM to mM) and its associated effects [7–10]. Cellular activation *in vivo* or presence of calcium *in vitro* allows either translocation of LOX from cytosol to membrane and/or altered enzyme activity to catalyze fatty acid substrate(s) [11–13]. In case of 11R-LOX from *Gersemia fruticosa*, the oxygenase activity could be observed in response to Ca^{2+} (50 μM) in presence of phospholipids, while ≈ 1.5 mM Ca^{2+} resulted in maximal activity [14].

LOXs have been structurally apportioned into two domains, a large C-terminal catalytic domain with prosthetic iron, and a smaller N-terminal also referred to as the PLAT (Polycystin-1, Lipoxygenase, α-toxin) domain. Due to limited success in getting crystal structures, comparisons to the C2-domain in $cPLA_2$ and the C2-like domain in *C. perfringens* α-toxin, have implicated residues in LOXs, as ligands to Ca^{2+} and membrane [15–17]. In fact mutagenesis in N-PLAT domain of LOXs has led to decreased Ca^{2+} binding or abolished activity and a

* Corresponding author at: Division of Chemistry 2, Department of Medical Biochemistry and Biophysics, Karolinska Institutet, 171 77 Stockholm, Sweden.
E-mail address: monica.mittal@ki.se (M. Mittal).

http://dx.doi.org/10.1016/j.bbagen.2017.05.015
Received 30 January 2017; Received in revised form 12 May 2017; Accepted 17 May 2017
Available online 19 May 2017

requirement for higher Ca^{2+} concentration to activate LOXs [18–20]. However for few others, a low binding affinity (dissociation constant, 0.2–0.5 nM) has also been proposed, suggesting the involvement of catalytic domain as well [8]. Thus, there is a great deal of variation in terms of binding of calcium and/or presence of specific binding sites. Interestingly, for both 8R-LOX from *Plexaura homomalla* and h5-LOX, basal activities have been observed in absence of divalent cations and Ca-stimulated activities are subject to substrate inhibition. This suggests that Ca^{2+} may attain a primary role in dictating LOX dynamics, further regulating its activity secondarily. In spite of ample literature on LOX:Ca^{2+} interaction, we still have no idea what exactly happens to the enzyme on binding calcium.

There are a few reports suggesting flexible nature of LOXs in solution under different conditions [21–25]. Also, some LOX structures show that the Ca^{2+}-binding sites are complex in tertiary structure, which suspects a cascade of conformational changes involved on calcium binding [26]. However, there is no study that has focused on exploring the effect of calcium binding on LOX dynamics. Calcium binding is a crucial event and its effects have been investigated in other calcium sensor proteins. The associated conformational changes that different proteins undergo on Ca^{2+} binding and their downstream response have been discussed [27–33]. Thus, it intrigued us to investigate the behavior of a unique vertebrate 12-LOX from zebra fish and explore its structural-functional aspects in response to calcium.

In past, Zebra fish (*Danio rerio*) has emerged as a suitable model for early vertebrate development, and a number of targeted mutations in the zebrafish genome led to phenotypic alterations that resemble human diseases [34]. A 12-LOX in Zebra fish has been cloned and knock down of this *zf*12-LOX enzyme showed its indispensability for embryonic development [35,36]. This makes it a very good candidate to study how *zf*12-LOX behaves in solution and how presence of calcium and/or deletion of putative calcium binding residues alter the biophysical and functional properties of enzyme. Here we aimed to characterize *zf*12-LOX and created a soluble and more stable version of the enzyme. The solution structure of *zf*12-LOX has been investigated. Then we describe that Ca^{2+} activates the oxygenase activity of soluble *zf*12-LOX and this is related to a conformational change of the protein structure as observed by SAXS and other biophysical techniques. In comparison to the homologous crystal structures, *zf*12-LOX is suggested to display an outward shift of the N-terminal PLAT domain w.r.t. catalytic domain, thus adopting an open-state. The region near the active site also remodels, where all these changes may provide an easy transit to the incoming substrate into active site. Further, the role for putative calcium regulatory site (site-2) has been discussed and the site-2 mutant is shown to have reduction in calcium induced enzyme activity and adopts a closed state in solution. This is a detailed investigation that links Ca^{2+} binding with the activity of LOX and can be extended to other enzymes as well.

2. Materials and methods

2.1. Chemicals, reagents and enzymes

The chemicals used were from the following sources: (5Z,8Z,11Z,14Z)-eicosa-5,8,11,14-tetraenoic acid (arachidonic acid), EDTA, imidazole and ampicillin from Gibco (Eggenstein, Germany); Carbenicillin, glycerol, calcium chloride (99.99%) and *E. coli* strain BL21 (DE3) was purchased from Qiagen (Hilden, Germany). Oligonucleotide synthesis was carried out by Genscript (New Jersey, USA).

2.2. Construction of soluble zf12-LOX and site-2 mutant

Lipoxygenases are known to have either less stability or mixed oligomers. In order to have good quality and homogenous protein(s), we introduced four point mutations of residues in *zf*12-LOX in order to create a soluble version. These mutations (F74G, I75S, S241A, C558A), involved in membrane insertion or in vicinity, were selected on the strategy similar to that adopted for human 5-LOX [37]. This obtained clone for *zf*12-LOX with point mutations has been referenced here as the soluble *zf*12-LOX. To identify the primary sequence conservation between *zf*12-LOX and other 12-LOX proteins, we performed a multiple sequence alignment (MSA) using ClustalW. We included 5 sequences of 12-LOXs from *Homo sapiens*, 1 LOX sequence each from *Mus musculus*, *Rattus norvegicus* and *Oryctolagus cuniculus* and 2 LOX sequences from coral *G. fruticosa* and *P. homomalla*. The regions of conservation in this alignment combined with the information available in literature were used to predict putative calcium-binding residues (Site-2) in *zf*12-LOX. Further, to investigate the role of site-2, we changed these residues (^{38}DtoL and $^{41–45}$GLDFC, based on MSA) in soluble *zf*12-LOX, to create a site-2 mutant enzyme. Both soluble *zf*12-LOX and the site-2 mutant proteins were then used for further studies in response to calcium.

2.3. Expression and purification of protein(s)

To express and purify soluble *zf*12-LOX and the mutant proteins, BL21 *Escherichia coli* cells carrying the plasmid *pET23a*-12-LOX were grown in Luria-Bertani broth containing ampicillin (75 μg/mL) at 37 °C. When the OD_{600} reached to 0.6, IPTG was added to final concentration of 0.1 mM and the cells were shaken overnight at 150 rpm, 20 °C. The harvested cells were resuspended in buffer containing 25 mM Tris (pH-8.0), 250 mM NaCl, 5% glycerol, lysozyme (37 μg/mL), DNaseI and a protease inhibitor tablet. The suspension was lysed by sonication at 4 °C. The resulting mixture was centrifuged at 20,000*g* for 20 min to remove cell debris. The supernatant was loaded onto an equilibrated Ni-NTA column and washed with 20–40 mM imidazole. 12-LOX was then eluted in Tris buffer (25 mM, pH 7.5) containing 250 mM NaCl, 5% glycerol and 250 mM imidazole. SDS-PAGE was performed to confirm the presence of a 75 kDa band. The fractions containing purified protein were pooled and concentrated in an Amicon pressure concentrator to the required concentrations. The purity of the protein was checked by SDS-PAGE (PhastGel™ Gradient 10–15) electrophoresis in Pharmacia PhastSystem High speed electrophoresis System. The proteins used for the SAXS studies were purified in 25 mM HEPES (pH 7.5) containing 250 mM NaCl and 5% glycerol. The concentration of the protein(s) was determined by measuring the absorbance at 280 nm in a UV spectrophotometer. Beer lamberts law: $A = \varepsilon * l * c$ was used to calculate the protein concentration from the absorbance (ε_{280} = 124,220 M^{-1} cm^{-1}).

2.4. Binding assay of soluble zf12-LOX with calcium

To calculate the binding constant of 12-LOX with calcium, we utilized microscale thermophoresis (MST) to monitor and quantify the bi-molecular interaction. For this we labeled the purified protein with a fluorescent label (NT-647). The label was covalently attached to the protein (NHS coupling) in buffer containing 25 mM HEPES buffer pH 8.0 containing 0.2 M NaCl and 5% glycerol. In order to get rid of excess dye and/or unlabeled protein, the labeled protein was purified. In the MST experiment, a fixed concentration of NT647 labeled 12-LOX was titrated against calcium ranging from 10 nM to 1000 μM. After an incubation of 2 min, the samples were loaded into MST NT.115 standard glass capillaries and the MST analysis was performed using the Monolith NT.115. The concentration of ligand (nM) was plotted on the X-axis and analyzed to calculate the K_D.

2.5. Activity assay with arachidonic acid

All reactions were carried out at room temperature (22 °C) with a Cary 100 Bio UV/VIS spectrophotometer. Assays were carried out in 50 mM

Tris buffer (pH 7.5) containing phosphatidylcholine (25 μg/mL), $CaCl_2$ (1 mM) and $MgCl_2$ (1 mM). The substrate, arachidonic acid, (AA) concentration was varied from 5 to 50 μM, and initiated by the addition of enzyme, as described below. AA solutions were stored in absolute ethanol, and diluted into assay buffer so that the total ethanol concentration in the kinetic assays was < 1.5%. Enzymatic reactions were initiated in a total volume of 100 μL by the addition of 0.2 mg/mL 12-LOX. In order to eliminate a lag phase and obtain initial rates of the human enzymes before auto inactivation occurred, the enzymes were pre-activated with 13-HPODE [38]. A solution of 13-HPODE ($\varepsilon = 2.3 \times 10^4\ M^{-1}\ cm^{-1}$ at 235 nm) was prepared and added to a final concentration of 25 μM to each kinetic assay [39]. Initial rates (< 15% conversion) were determined by monitoring the formation of the conjugated product (12-HETE & 12-HpETE) at 235 nm ($\varepsilon = 2.25 \times 10^4\ M^{-1}\ cm^{-1}$) for each substrate concentration [1]. Same sets of experiments were repeated in the absence of $CaCl_2$ in the assay buffer. Kinetic data was then analyzed to determine the specific activity.

2.6. Quantification of 12-HETE by mass spectrometry (MS)

To determine the amount of product formed in the enzymatic reactions, the enzyme assays were done as explained above and quenched with 100 μL of methanol after 1 min. Then 50 μL of the reaction mixture was injected and analyzed in HPLC system (Waters 2695). A Phenomenex Luna C_{18} column was used and eluted with acetonitrile/water/acetic acid in the ratio 60:40:0.1. The results were analyzed and the amounts of 12-HETE were determined.

2.7. Circular dichroism (CD) studies

CD measurements were carried out with a JASCO spectropolarimeter (Jasco, Tokyo, Japan), equipped with a Peltier type temperature controller (PTC-348W). Far-UV spectra were obtained using a quartz cuvette with a 10 mm light path-length and each spectrum obtained was an average of 5 scans in the absence and presence (1 mM) of calcium. The ellipticity of protein CD spectra is reported as mean residue ellipticity (MRE) in deg/cm^2/dmol units. For all cases, the spectrum of buffer was subtracted to obtain the real protein spectra. Deconvolution of far UV-CD spectra was performed using Spectra Manager, software provided by the manufacturer (Jasco). The calculation of secondary structure content was done as mentioned earlier.

2.8. Thermostability analysis

Temperature-dependent aggregation was measured using Stargazer, Harbinger Biotech, Toronto, Canada [40,41]. Fifty microliters of protein (0.4 mg/mL) was heated from 20 °C to 80 °C at a rate of 1 °C per min in each well of a clear-bottom 384-well plate (Nunc, Rochester, NY) in the absence and presence of calcium (1 & 5 mM). Incident light was shone on the protein drop from beneath at an angle of 30°. The protein aggregation was monitored by measuring the intensity of scattered light, every 30 s, with a CCD camera. The pixel intensities in a preselected region of each well were integrated to generate a value representative of the total amount of scattered light in that region. These total intensities were then plotted against temperature for each sample well and fitted to the Boltzmann equation by nonlinear regression. The resulting point of inflection of each resulting curve was defined as the T_{agg}. Xylanase (Roche, Indianapolis, IN), a commercially available protein with well defined properties, was used as a standard to determine the reproducibility of the observed T_m [42] and a standard deviation of 0.4 °C was determined in the T_{agg} for three independent measurements.

2.9. Size exclusion chromatography

To characterize oligomeric states of the purified protein(s) (both soluble and site-2 mutant), size exclusion chromatography was performed using HiLoad™ 16/60 Superdex™ 200 column. The column was equilibrated using Buffer containing 25 mM Tris-HCL (pH 7.5), 250 mM NaCl and 5% glycerol). The individual proteins were injected at a concentration of 5 mg/mL and eluted at a flow rate of 1 mL/min. In order to have stable protein-ligand complex, the proteins were incubated with $CaCl_2$ (approx. 1000 times the K_D to ensure full occupancy in solution), mixed immediately, filtered and injected to the column. The fractions containing the protein(s) were concentrated using a 50 kDa Millipore Amicon Ultra-15 centrifugal filters and stored in − 80 °C. The corresponding peaks were compared with the standard markers pre-run on the column to determine the MW of the purified proteins.

2.10. Dynamic light scattering

Dynamic light scattering measurements were performed at the temperature of 20 °C using a 3000 HSA Zeta-Sizer (Malvern) apparatus equipped with 512 channels. An He-Ne laser was used with power of 45 mW and the scattering angle was equal to 90°. Measurements were performed with a 100 μm aperture using quartz cuvette containing 100 μL of sample in a thermostated cell holder. During experiments, 100 μL filtered protein solution was placed into DLS cells and $CaCl_2$ was added to it (1 & 5 mM). The solutions were mixed and the measurements were initiated within 30 s after mixing. Duration of a single experiment was 210 s, which allowed us to probe the progress of the binding process undergoing in the solution. The individual autocorrelation spectra were analyzed to calculate the hydrodynamic radius (R_h^0) and the apparent molar mass (M).

2.11. Small angle X-ray scattering (SAXS)

2.11.1. SAXS data collection

We performed preliminary SAXS experiments at I911-SAXS beamline at the MAX IV laboratory, Lund, Sweden [43] and BioSAXS beamline, BM29, ESRF, Grenoble, France [44]. These experiments helped in testing the conditions for longer protein stability, minimum aggregation and any radiation damage. The data presented here was finally collected at the synchrotron beam line P12, EMBL (Deutsches Elektronen-Synchrotron), Hamburg, Germany. For soluble *zf*12-LOX and the site-2 mutant, on-line size exclusion chromatography with SAXS (SEC-SAXS) was employed to obtain scattering data, where 5 mg/mL purified sample was loaded onto HiLoad 10/300 GL Superdex S200 (GE Healthcare) column. The protein(s) were eluted at a flow rate of 0.3 mL/min and passed through the capillary cell with frames collected every 1 s with a total of 3000 frames.

To collect data for the calcium bound enzyme, *zf*12-LOX protein samples were incubated with $CaCl_2$ (1 mM) for 5 min before data collection. All the samples were centrifuged, filtered and the protein concentrations were determined by A_{280} measurements using a Nanodrop Spectrophotometer (Thermo Scientific) using a molar extinction coefficient of 124,220 $M^{-1}\ cm^{-1}$ as calculated from Protparam [45]. The protein solutions were circulated slowly in the measuring quartz capillary (diameter 1.5 mm) to avoid any possible protein damage due to X-ray irradiation and the temperature was kept constant at 10 °C. The scattered intensities were recorded on a pixel detector, Pilatus 2 M (Dectris Ltd.) using a position-sensitive proportional detector, at a sample-detector distance allowing the range of momentum transfer q from 0.022 nm^{-1} to 4.28 nm^{-1} ($q = 4\pi \sin \Theta/\lambda$, where 2q is the scattering angle and λ is the wavelength of the X-rays) to be covered. Twenty frames of 45 ms each were recorded and compared to each other to check for any radiation damage. The monodispersity of the protein samples were measured by dynamic light scattering using a

Table 1
SAXS data collection, processing and scattering derived parameters.

Data-collection parameters	Soluble *zf*12-LOX	Soluble *zf*12-LOX + Ca^{2+}	Site-2 mutant	Site-2 mutant + Ca^{2+}
Beamline	P12, Hamburg	P12, Hamburg	P12, Hamburg	P12, Hamburg
Wavelength (nm)	0.123987	0.123987	0.123987	0.123987
q range (nm^{-1})	0.022–4.82	0.022–4.82	0.022–4.82	0.022–4.82
Exposure time (seconds)	0.045	0.045	0.045	0.045
Protein concentration (mg/ml)	5.0*	5.0	5.0*	5.0
Temperature (K)	283.15	283.15	283.15	283.15
Structural parameters				
I(0) (cm^{-1}) [from Guinier/*P*(*r*)]	5446 ± 45/5435 ± 64	8194 ± 12/8329 ± 29	4829 ± 34/4925 ± 61	9048 ± 12/9279 ± 43
R_g (nm) [from Guinier/*P*(*r*)]	2.90 ± 0.04/2.94 ± 0.04	3.24 ± 0.03/3.28 ± 0.03	2.90 ± 0.03/2.94 ± 0.04	3.20 ± 0.02/3.27 ± 0.02
D_{max} (nm)	10.08 ± 0.2	13.31 ± 0.1	10.02 ± 0.2	13.18 ± 0.1
Porod volume estimate (nm^3)†	121.43	127.39	122.01	113.11
Dry volume calculated from sequence (nm^3)	93.44	93.44	93.44	93.44
Molecular-mass determination				
Calculated monomeric M_r from sequence [kDa]	77.01	77.01	77.01	77.01
Molecular mass from excluded volume (kDa)‡	73.03	86.00	84.80	82.73
Softwares employed				
Data processing	*Primus*	*Primus*	*Primus*	*Primus*
P(*r*) function calculation	*GNOM*	*GNOM*	*GNOM*	*GNOM*
Three-dimensional graphics representations	*PyMOL*	*PyMOL*	*PyMOL*	*PyMOL*
Modeling parameters				
Ab-initio analysis	*GASBOR*	*GASBOR*	*GASBOR*	*GASBOR*
Validation and averaging	*DAMAVER*	*DAMAVER*	*DAMAVER*	*DAMAVER*
χ^2	0.77 ± 0.002	1.04 ± 0.020	0.65 ± 0.011	1.00 ± 0.022
NSD	0.92 ± 0.057	1.12 ± 0.063	0.92 ± 0.059	1.02 ± 0.058

Zetasizer Nano-ZS (Malvern) instrument and the datasets were analyzed using inbuilt software. Further details are provided in Table 1.

2.11.2. SAXS data processing

The datasets collected for the different protein concentrations were compared to each other in order to examine any aggregation. The datasets were then processed and scaled using program Primus [46]. The radius of gyration (R_g) of the proteins in solution was determined from the lowest q values of the SAXS data, using the approximation:

$$I(q) = I(0)\exp(-R_g^2 q 2/3)$$

valid over a restricted q-range (typically $R_g q < 1.3$) [47]. The value I(0)/c, the scattering intensity at zero angle normalized to the protein concentration of the sample, is proportional to the molecular mass M of the protein, which can be estimated after proper calibration of the intensity using reference samples. The distance distribution function, representing the distribution of distances between any pair of volume elements within the particle, together with the structural parameters derived from *P*(*r*), *i.e.* the maximum dimension of the particle (D_{max}), and the radius of gyration, were evaluated using the indirect transform method as implemented in the program GNOM [48,49].

2.11.3. Ab initio modeling and comparison with homologs

The model calculations were performed by GASBOR [50] and DAMMIN [51]. For both calculations the scattering profiles more than $q_{max} = 2.1\ nm^{-1}$ were used and 15 repetitive runs of modeling were carried out with each method. The obtained models per sample, 15 each for soluble *zf*12-LOX and the site-2 mutant in the presence and absence of calcium, were averaged and filtered using DAMAVER [52]. As an additional check on the oligomeric state of 12-LOX in response to calcium, GASBOR and DAMMIN, several *ab-initio* dummy residue reconstructions were performed assuming monomeric as well as other oligomeric organizations. In all cases the models were built assuming that either symmetry or no symmetry was present. Although the LOX overall structure is highly conserved, however there is no full-length crystal structure available for 12-LOX. Based on our MSA results and phylogenetic analysis, human 5-LOX appears to be the closest homologue of *zf*12-LOX. Also this was confirmed by CRYSOL analysis of the scattering curves with several available homologue crystal structures to LOXs [55]. Thus we selected crystal structure of human 5-LOX for comparison analysis with the obtained *ab initio* models. Further details about data processing are presented in Table 1.

3. Results

3.1. Prediction of putative calcium responsive residues and characterization of soluble zf12-LOX and site-2 mutant in zf12-LOX

The soluble version of the *zf*12-LOX was created as explained in materials and methods section and purified from *E. coli*. The wild type and soluble *zf*12-LOX enzymes were compared and higher melting temperature for soluble *zf*12-LOX clearly showed that it is more stabilized in solution compared to wild type (Supplementary Fig. S1). The activity of the soluble *zf*12-LOX was compared with that of the wild-type *zf*12-LOX (without point mutations). The results clearly showed that the activity and calcium dependency for soluble *zf*12-LOX was found to be very similar to that of wild type *zf*12-LOX (Supplementary Fig. S2), thus ruling out any major alteration in enzymatic properties. This ensures that the point mutations introduced to create soluble *zf*12-LOX *in vitro* do not affect the protein in terms of activity and response to calcium.

The results of our sequence alignment highlighted 2 main regions of conservation, one common to all sequences, corresponding to the loop region 1 in LOXs. The residues in N-PLAT domain, especially the loop regions in LOXs, have been shown to deliver Ca^{2+} mediated responses and bind calcium through either backbone or side chain interactions. Some of these residues (in 15-LOX-2, 5-LOX, coral 8R-LOX) have been mutated, with effects on Ca^{2+} binding or Ca^{2+} activation of enzyme activity [25]. A second region of conservation, corresponding to site-2 was clearly identifiable in R-type LOXs and absent in S-type LOXs. Interestingly *zf*12-LOX has some of these residues, thus suggesting that the stretch might be involved in Ca^{2+} responsive effects of *zf*12-LOX (Fig. 1). To investigate the role of this site-2 stretch in *zf*12-LOX, we created a site-2 mutant enzyme. Recombinant full-length site-2 mutant proteins were purified from *E. coli*. The SDS-PAGE analysis showed a

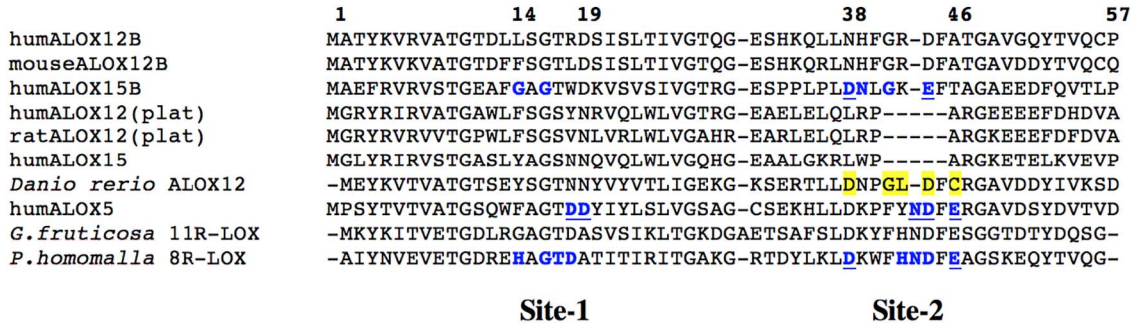

Fig. 1. Multiple sequence alignment of *zf*12-LOX with other LOXs, highlighting the calcium-interacting residues in ligand binding loops; site 1 (residues: 14–19) and site-2 (residues: 38–46). The residues (mentioned at the top of alignment) have been numbered according to the NCBI records for *zf*12-LOX. **Blue, bold** indicates residues binding Ca^{2+} *via* side chains/backbone, in crystal structures. In 5-LOX **bold** indicates residues impacting on Ca^{2+} activation of 5-LOX. Underlined residues have been mutated, with effects on binding of Ca^{2+}, or Ca^{2+} induced enzyme activity. The residues mutated in *zf*12-LOX site-2 are highlighted in yellow.

clean band at around 75 kDa for both soluble *zf*12-LOX and the site-2 mutant and the final enzyme preparations exhibited a high degree of purity (> 95%).

3.2. *zf12-LOX exists as a monomer in solution and the oligomeric state is unaltered in the presence of calcium*

To characterize the oligomeric state(s) of proteins, size exclusion chromatography (SEC) was performed in the absence and the presence of calcium. A K_D value of *zf*12-LOX for Ca^{2+} was estimated to be ~10 μM by microscale thermophoresis (Fig. 2A).

The purified wild type enzyme was highly unstable and non-homogenous in solution. Thus SEC was performed in presence of 1 mM Ca^{2+} (to ensure full ligand occupancy in solution) for both soluble *zf*12-LOX and site-2 mutant proteins. The SEC profile for soluble *zf*12-LOX showed a peak eluting at ~80 mL. Following incubations with calcium (1 mM) for 15 min preceding SEC, the elution profile showed a peak at ~76 mL (Fig. 2B–E). For the site-2 mutant, the elution volumes were ~81 and ~79 mL in the absence and presence of calcium respectively. The data were plotted as partial specific volume (K_{av}) and log molecular weight (MW) making it independent of the chromatography conditions (Fig. 2D). When compared to the standard proteins of known MW, the molecular species in solution corresponds to that of ~77 and ~69 kDa for soluble enzyme and the site-2 mutant respectively, irrespective of the calcium. This shows that both soluble *zf*12-LOX and site-2 mutant exist as a monomer in solution and there is no change in the assembly state in the presence of calcium.

3.3. *zf12-LOX displays increase in enzyme activity in the presence of calcium*

To assess the enzyme activity of soluble *zf*12-LOX, we used arachidonic acid (AA) and linoleic acid (LA) as substrates. The apparent K_M for AA was lower, and thus this fatty acid was used in subsequent assays. Addition of Ca^{2+} (1 mM) increased the activity of soluble *zf*12-LOX. The effect of Ca^{2+} depended on the AA concentration, reaching a maximum at 100 μM AA (phosphatidylcholine was 25 μg/ml) (Fig. 3A). The kinetics revealed pronounced substrate inhibition at higher AA in presence of Ca^{2+}, precluding calculation of Michaelis-Menten parameters, which also rules out the possibility of auto-oxidation. The increase in activity was ~2.5 fold at 25 μM in the presence of Ca^{2+} (1 mM), however reaching to a maximum of ~10-fold at AA conc. > 50 μM. However, it might circumvent the micelle formation at A-A > 50 μM, thus the values at lower AA are considered more appropriate. The site-2 mutant exhibited only slight change in activity as compared to soluble *zf*12-LOX in the absence of calcium (Fig. 3B). Contrarily it significantly lost the increase in activity in the presence of calcium. The specific the specific activity of soluble *zf*12-LOX is increased by nearly 75% (25 nmol/min/mg) in the presence of calcium as compared to that in its absence (7 nmol/min/mg). However for the site-2 mutant, it is 5 nmol/min/mg irrespective of the presence of calcium. Thus it suggests that site-2 residues are involved in regulating calcium-mediated response of enzyme.

We also monitored the complete product profiling by mass spectrometry that showed no change in reaction specificity of either enzymes. We quantified the 12-HETE formation by MS-MS also, showing ~2.5-fold increase for soluble *zf*12-LOX and no change in site-2 mutant in the response to calcium (Supplementary Fig. S3). Thus, it shows that the calcium and site-2 residues regulate the enzyme activity under physiologically favorable conditions for the substrate.

3.4. *Ca^{2+} decreases the aggregation temperature of soluble zf12-LOX, while secondary structure is maintained*

The effect of calcium on protein stability was determined by a thermostability assay. The average aggregation temperature (T_{agg}) for soluble *zf*12-LOX was 58 ± 0.4 °C and shifted to 53 ± 0.6 °C in the presence of calcium (1 mM). This decrease in T_{agg} for soluble *zf*12-LOX in response to calcium suggests that the two (unbound and bound) states are conformationally different from each other. Similar experiment for the site-2 mutant protein gave T_{agg} of 48 ± 1.0 °C and 49 ± 0.5 °C in the absence and presence of calcium (1 mM) respectively or even higher ligand concentration (Fig. 4A, B). This shows that the soluble *zf*12-LOX enzyme is fairly stable under the conditions used in this study and the mutant protein is comparatively less stable. However, the site-2 mutant is not affected substantially by the presence of calcium.

In order to check for any change in secondary structure responsible for enzymatic instability in the presence of calcium, we performed the CD spectroscopy. The ellipticity plots show that the soluble *zf*12-LOX as well as site-2 mutant enzymes encompass ~25% helix and ~35% sheets and adding calcium (1 mM) does not show any remarkable change in secondary structure (Fig. 4C). This shows that the structural integrity of both enzymes is maintained irrespective of calcium.

3.5. *Presence of Ca^{2+} induces increase in molecular dimensions of soluble zf12-LOX*

To investigate any change in biophysical parameters of *zf*12-LOX, we performed Dynamic light scattering (DLS) experiments. The results showed a smooth decay in autocorrelation function (ACF) for both the proteins, which was used to extract particle size. The data was deconvoluted to calculate the hydrodynamic radius (R_h), that came out to be 2.8 and 2.6 nm for *zf*12-LOX and the site-2 mutant

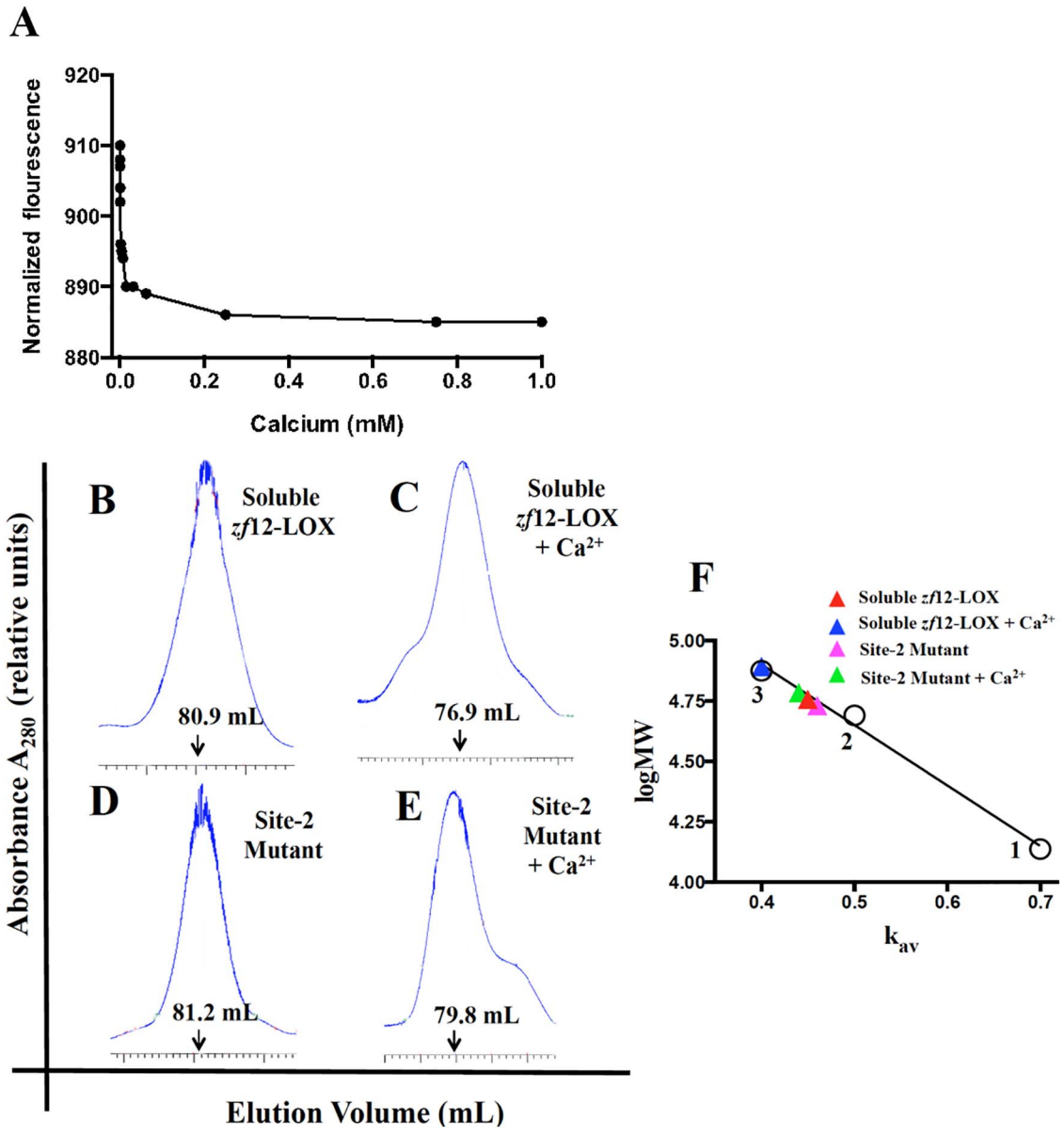

Fig. 2. (A) Determination of K_d for *zf*12-LOX and calcium using the Monolith® NT.115^{Pico}. Titration of the non-fluorescent ligand results in a gradual change in thermophoresis, which is plotted as normalized fluorescence to yield a binding curve, which is fitted to derive binding constants. Lower left panel shows size exclusion chromatography (SEC) showing the elution volumes for (B) soluble *zf*12-LOX, (C) soluble *zf*12-LOX in the presence of calcium, (D) site-2 mutant and (E) site-2 mutant in the presence of calcium. (F) Lower right is the calibration plot showing corresponding molecular weights *vs* partition coefficient ($^*K_{av}$) for standards (open circles) and the *zf*12-LOX proteins as mentioned (closed triangles). The standards used here, 1 - Ribonuclease A (13.7 kDa), 2 - Ovalbumin (45 kDa) and 3 - Conalbumin (75 kDa) respectively.

$^*K_{av} = V_e - V_o/V_c - V_o$

where V_e = elution volume, V_o = void volume and V_c = column volume.

respectively. This clearly shows that the mutant is slightly smaller in size. Interestingly, the ACF curve shifted on adding calcium, suggesting presence of bigger particles in solution (Fig. 5A). The R_h was calculated to be 3.15 and 2.9 nm on calcium binding for *zf*12-LOX and the site-2 mutant respectively. These changes were observed with 1 mM Ca^{2+}, and were practically the same with 5 mM Ca^{2+} (Fig. 5B).

Interestingly, the polydispersity index (PDI) did not show any significant change for any of the samples suggesting that the protein (s) majorly exist as single species in solution (not shown here). The average molecular weight calculated (from R_h values) corresponds to that of a monomer for both enzymes irrespective of calcium. This suggests that although there is no oligomeric change but *zf*12-LOX encompasses globular rearrangements resulting in increased molecular dimensions on adding calcium.

3.6. SAXS shows increase in R_g and D_{max} of zf12-LOX in the presence of Ca^{2+}

The SAXS scattering profiles show that all the samples were well behaved in solution and did not show any inter-particle repulsion or aggregation (Fig. 6A–D). The linear Guinier plot (inset Fig. 6A–D) indicates that the aqueous solution was monodisperse, and the scattering solutes yielded a radius of gyration R_g of 2.91 ± 0.03 and 2.90 ± 0.02 nm for soluble *zf*12-LOX and the site-2 mutant protein respectively. The volume of the scattering solutes (mentioned in Table 1) corresponds to a molecular mass of 73 ± 5 kDa, which is similar to that of theoretical monomer (75 kDa). These results confirm the presence of soluble *zf*12-LOX and site-2 mutant as monomers in solution.

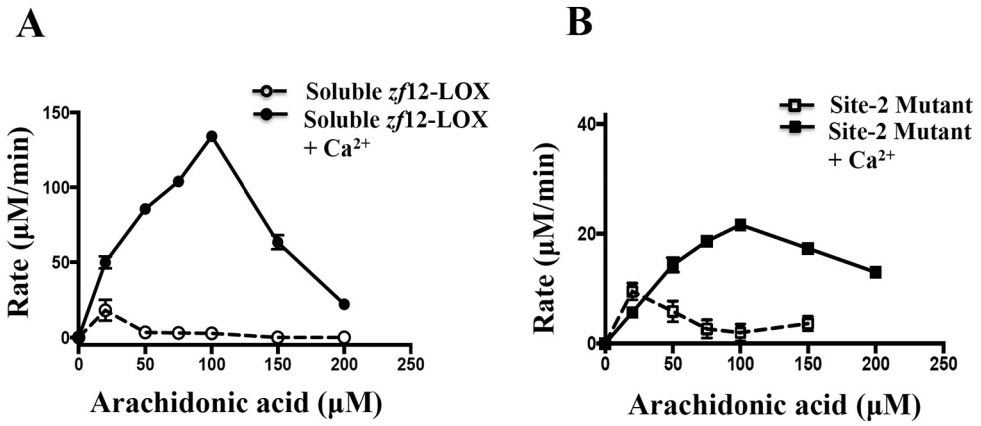

Fig. 3. Steady state kinetics with arachidonic acid (AA) in the absence and presence of calcium for (A) soluble *zf*12-LOX and (B) site-2 mutant using UV–Vis spectrophotometer.

The pairwise distribution function, $P(r)$ calculated from the scattering data shows a single peak and the maximum diameter (D_{max}) of the solute particles was estimated to be 10.08 ± 0.2 and 10.02 ± 0.2 nm for soluble and the site-2 mutant protein respectively (Fig. 6E). The distribution has a maximum at near $D_{max}/2$ suggesting that the molecules are symmetrical in solution. In the presence of calcium, the R_g value changed to 3.24 ± 0.03 and 3.18 ± 0.05 nm and the D_{max} was estimated to be 13.31 ± 0.02 and 13.18 ± 0.05 nm for soluble and the site-2 mutant protein respectively. The increase in dimensions suggests presence of bigger particles in presence of calcium. Since the decrease in $P(r)$ to D_{max} is smooth, thus this increase is due to inherent shape of protein and not due to aggregation. Extensive unfolding of the enzyme was overruled by bell-shaped Kratky plots [q^2I (q) *versus* q] (Supplementary Fig. S4), thus exhibiting the characteristics of a properly folded protein. Estimating the hydrated volume of globular proteins, we obtained the molecular mass estimate of ~86 kDa in the

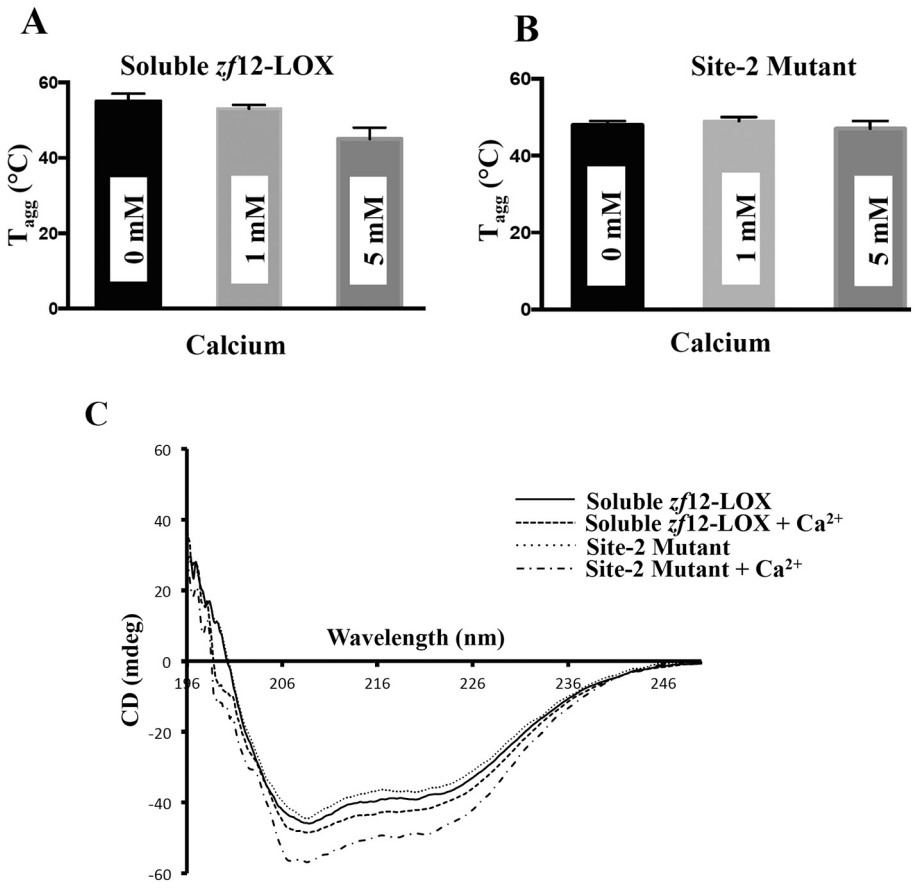

Fig. 4. Thermostability plots showing the change in T_{agg} for (A) soluble *zf*12-LOX and (B) site-2 mutant protein in the absence and presence of calcium as stated in the figure. (C) CD spectra showing the secondary structure content of soluble *zf*12-LOX and the site-2 mutant in the absence and presence of calcium as described in figure.

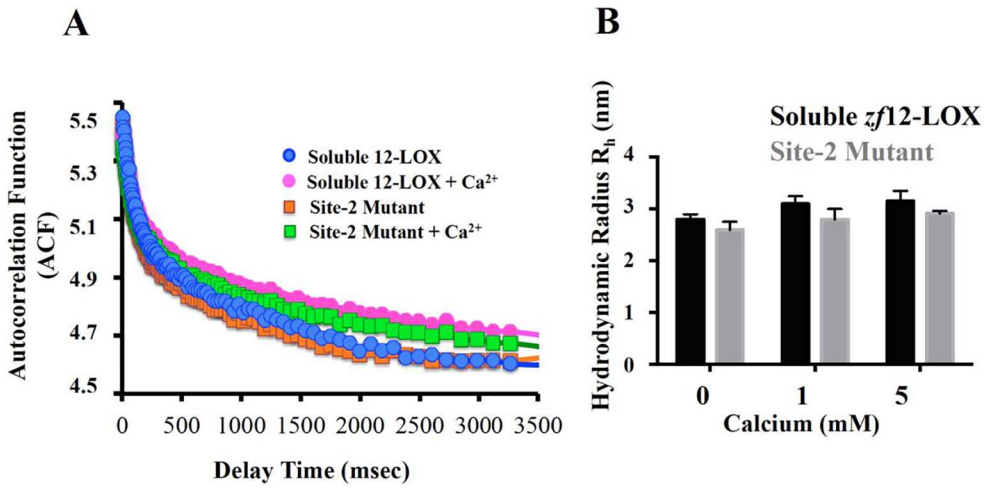

Fig. 5. (A) Auto correlation spectra of soluble *zf*12-LOX and the site-2 mutant protein in the absence and presence of calcium monitored by Dynamic light scattering. The spectra shift in response to calcium for both soluble *zf*12-LOX and the site-2 mutant. (B) Hydrodynamic radius (R_h) is plotted in the absence and presence of calcium for soluble *zf*12-LOX and the site-2 mutant showing increase in the presence of calcium.

presence of calcium.

Interestingly the long tailing of the *P*(*r*) peaks with a maximum at less than $D_{max}/2$, suggests that the soluble *zf*12-LOX monomer is an elongated species with a protruding part in the presence of calcium. In case of site-2 mutant, the *P*(*r*) distribution is slightly skewed towards the trailing end for the mutant, reflecting a non-similar shape. These data suggest a different degree of motional flexibility for both the proteins. The most likely interpretation for the observed structural differences is probably due to re-arrangement of protein-domains relative to each other. Thus, presence of calcium caused major alterations not in monomer size but shape. These differences prompted us to further explore the structural flexibility of both enzymes employing *ab-initio* modeling.

3.7. Solution structure of zf12-LOX structure in the absence and presence of calcium

To obtain more specific structural information, *ab initio* modeling methods (DAMMIN and GASBOR) were applied independently to reconstruct the overall shape from X-ray scattering data. The independent reconstructions yielded very similar shapes, as shown by the low value of normalized special discrepancy (NSD), calculated with DAMAVER program package. The averaged models fitted to the experimental data with good statistical agreement (Table 1, Supplementary Table 1).

The overall shape of soluble *zf*12-LOX looks ellipsoidal in shape that undergoes significant re-modeling on adding calcium, resulting in a more elongated and arched shape (Fig. 7A, B). The difference in the scattering envelopes for the two states is shown in a superimposed state (Fig. 7C). The differences clearly show the regions afflicted by conformational changes in response to calcium. In case of site-2 mutant, the overall shape is more oblate and looks more spread out in lower part of the molecule. Addition of calcium allows some movement but restricts it to adopt a shape similar to that of *zf*12-LOX (Fig. 7D, E). The superimposed densities for site-2 mutant in the absence and presence of calcium clearly show very limited amount of motion (Fig. 7E). The superimposed models are shown in perpendicular directions to clearly explain the difference in shapes in solution (Supplementary Fig. S5).

3.8. Conformational changes of zf12-LOX in solution in response to calcium

Currently no structure is available for full length 12-LOX containing multiple domains. To gain structural insight into *zf*12-LOX, we performed SAXS experiments and calculated it low-resolution molecular envelope. The *ab-initio* low-resolution molecular shape calculated by GASBOR shows an ellipsoidal envelope where two lobes are clearly distinguishable (Fig. 7), a larger one with a length of 0.6 nm and a smaller one with a length of 0.3 nm. To date, the closest structural homologue for *zf*12-LOX is human 5-LOX. Therefore we used the coordinates of h5-LOX to evaluate its solution scattering profile and compared to the experimental curve of *zf*12-LOX by program SUPCOMB [54]. The fitting of *zf*12-LOX SAXS data, measured at 5 mg/mL, with the structures of h5-LOX are shown in Supplementary Fig. S6 and Figure 8A and B.

The comparison of scattering patterns and the model (PDB: 3o8y) indicates that the overall organization of soluble *zf*12-LOX is very similar to h5-LOX (χ^2 = 1.12). The two lobes, corresponding to large catalytic and small N-PLAT domain, appear to be in close vicinity to each other, thus adopting the compact state of h5-LOX. In contrast, the calcium-bound solution state of *zf*12-LOX fits better to the coordinates of h5-LOX complexed with arachidonic acid (AA) (PDB: 3v99). The comparison suggests that *zf*12-LOX + Ca^{2+} structure in solution differs from the semi-open state of crystal template (χ^2 = 4.16). The solution structure of *zf*12-LOX + Ca^{2+} appears to be more flexible and the regions corresponding to N- and C-domains are stretched out and are arranged far apart from each other as compared to that in h5-LOX + AA crystal state. Such transition may not be readily visible in X-ray structures of h5-LOX due to packing constrains and high solute concentration. Thus, the compact and extended states observed here for the soluble *zf*12-LOX in the absence and presence of calcium, represent the closed and open conformation of zf12-LOX. Similar calculations were performed for site-2 mutant. The fitting of site-2 mutant SAXS data at same concentration is more restricted and there is less pronounced change for Ca^{2+} leading to relative domain positioning (Fig. 8C and D). Thus, site-2 mutant displays a lower degree of freedom and adopts a closed state. These results suggest how calcium can influence different protein-state transitions and the role of putative calcium-binding residues in regulating this dynamics.

4. Discussion

Among several factors that can regulate LOXs, transfer from cytosol to membranes is a common property for most of the enzymes in the family [8,18,56]. Ca^{2+} has been a pre-requisite for membrane binding

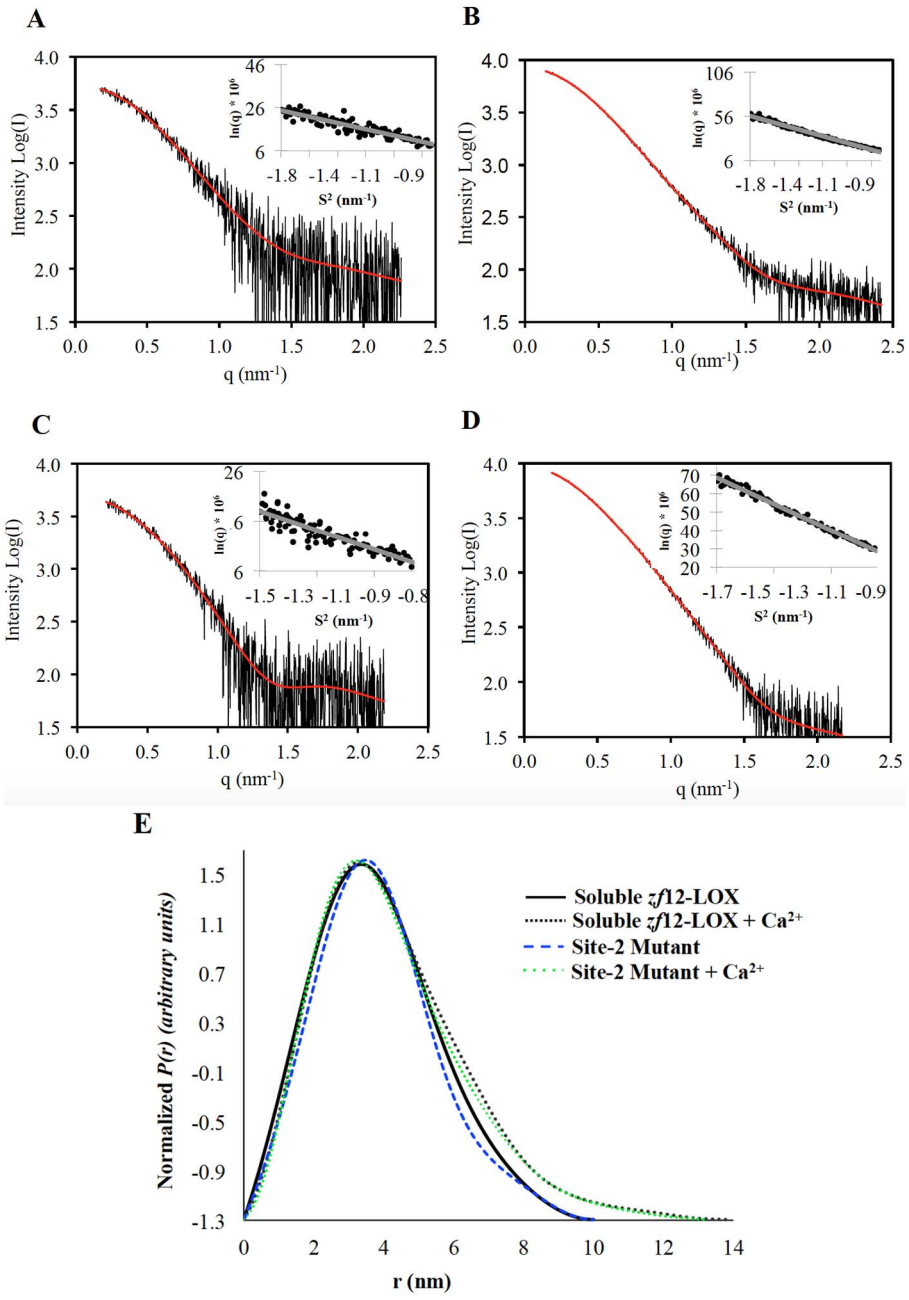

Fig. 6. X-Ray Scattering profiles and the representative Guinier plots (in inset) for (A) soluble *zf*12-LOX, (B) soluble *zf*12-LOX + Ca^{2+}, (C) site-2 mutant and (D) site-2 mutant + Ca^{2+} respectively.

(E) Inter atomic length distribution *P*(*r*) plots for soluble *zf*12-LOX and the site-2 mutant protein in the absence and presence of calcium are shown. An increase of 0.33 nm R_g and 3.23 nm D_{max} of soluble *zf*12-LOX; and 0.28 nm and 3.16 nm D_{max} of site-2 mutant was observed upon Ca^{2+} binding. For comparison, the values for soluble *zf*12-LOX + Ca^{2+}, site-2 mutant and the site-2 mutant + Ca^{2+} were corrected to a factor of 0.281, − 0.085 & − 0.261 respectively with respect to the soluble *zf*12-LOX.

and thus activity, as described in many cases both *in vitro* and *in vivo*. However, very few studies have addressed the effects of Ca^{2+} on LOX physical properties and the conformational changes that the enzyme may undergo upon Ca^{2+}-binding. In this study, we found that the oxygenase activity of *zf*12-LOX is up-regulated by Ca^{2+} in presence of phosphatidylcholine. We generated a stabilized form of *zf*12-LOX protein by exchange of four residues (F74G, I75S, S241A, C558A), which was also activated by Ca^{2+}. On comparing the sequence alignments for known Ca^{2+} activated LOXs, *zf*12-LOX shows a 'site-2' stretch containing putative Ca^{2+} binding residues. Mutagenesis of site-2 residues rendered the enzyme less active in presence of Ca^{2+}, thus indicating a potential role in Ca^{2+} regulation of enzyme catalysis. The K_D for binding of Ca^{2+} to soluble *zf*12-LOX was estimated as 10 ± 2 μM, similar to values reported for 5(*S*)-LOX [16]. The observation that the site-2 mutant is less active than its soluble counterpart is intriguing. There was no change in secondary structure (CD spectroscopy), or the oligomeric state as seen earlier for some LOXs earlier [21]. However, the reduced maximum activity of the site-2 mutant suggests '*action at a distance*' behavior.

Our in-solution studies provide an evidence for the above effect. Although the R_h and R_g values are similar for soluble *zf*12(*S*)-LOX and the site-2 mutant proteins, the pair distribution *P*(*r*) profiles and *ab-*

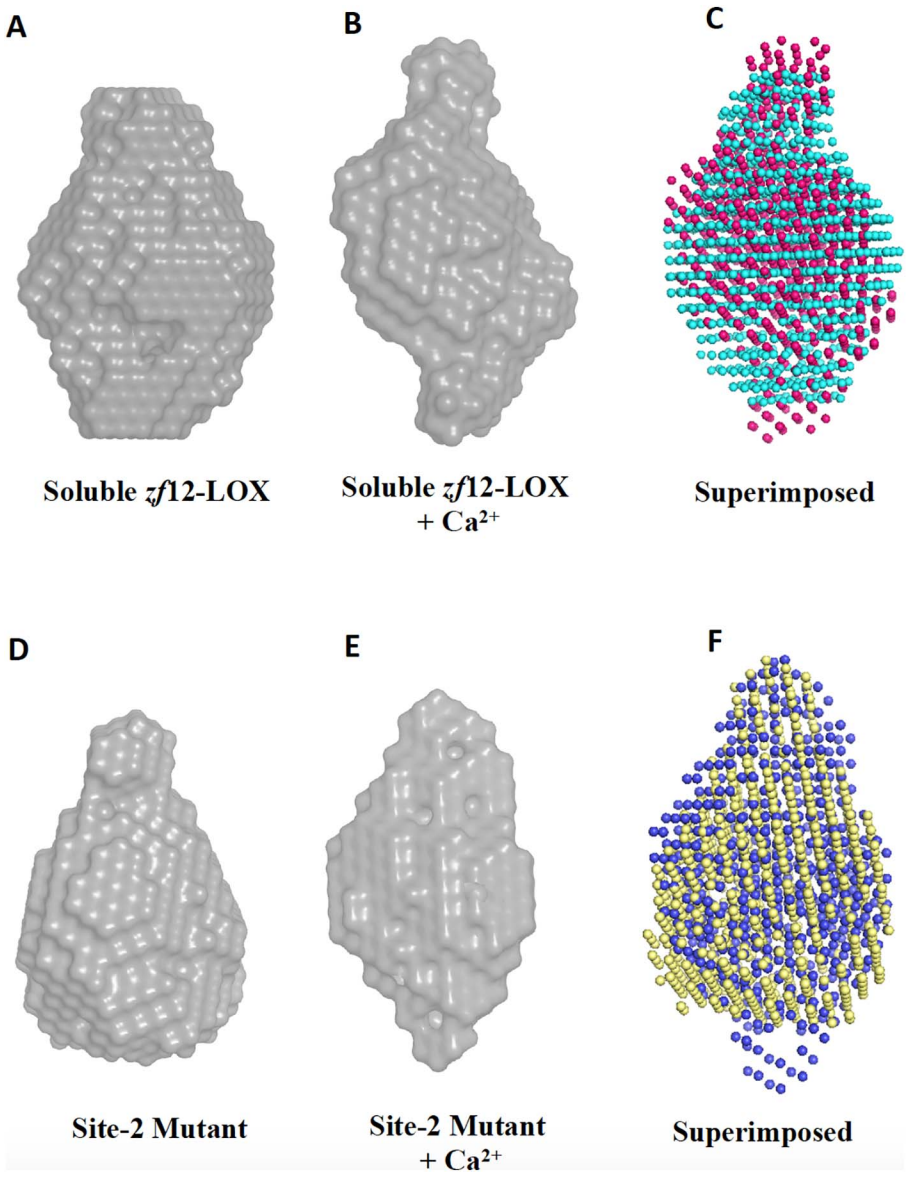

Fig. 7. *Ab initio* shape reconstruction showing space filling models (front view) of SAXS solution structures of *zf*12-LOX (A, B) and site-2 mutant (D, E) in the absence and presence of calcium. Superimposition of shapes (bead model) showing differences for (C) soluble *zf*12-LOX (cyan) and soluble *zf*12-LOX + Ca^{2+} (pink) and (F) site-2 mutant (yellow) and site-2 mutant + Ca^{2+} (blue). All figures were made in Pymol [53].

initio modeling clearly indicate the differential mass distributions in space. The observed differences in solution envelopes could be compared with the probable movements that the enzyme experiences w.r.t. the template. The Ca^{2+}-induced movements are more pronounced in soluble *zf*12-LOX, which was also supported by the evident decrease in transition temperature (thermostability assay) in response to calcium. Mutation of site-2 residues shows a rather more rigid state of mutant protein, thus suggesting that this might govern the re-positioning of N-PLAT and catalytic domains, directly or indirectly through calcium. The Ca^{2+} induced movements of the N-PLAT and catalytic domain regions are very different in the model structures of soluble *zf*12-LOX and the site-2 mutant, resulting in distinct '*open*' and '*closed*' states in the absence and presence of Ca^{2+}. Additionally the remodeling dynamics has also been observed in the center region of the solution envelopes of *zf*12-LOX that corresponds to the active site of the enzyme (Fig. 8). Previous studies have suggested that the α2-helix region near the active site acts as a "lid" in an otherwise open active site [26,57,58]. This suggests that calcium binding to the N-domain may allow *zf*12-LOX to adopt a state more accessible for the substrate (AA) into the active site in C-catalytic domain. Fiddling with the site-2 residues renders the protein trapped in a more 'closed state', resistant to Ca^{2+} induced transitions, also seen in case of decrease in calcium dependent activity of site-2 mutant. Thus, our study supports the concept of multiple conformations as reviewed for many other LOXs [59,60]. We also provide an explanation for the possible allosteric connection between the N- and C-terminal domains of *zf*12-LOX region in response to calcium that can be extended to the exposure of putative substrate entrance channels and altered enzyme activity.

5. Concluding remarks

Enhanced membrane binding upon calcium stimulation in cells suggests a pre-requisite step that involves a conformational change in LOX. This might facilitate it to tether to the membrane and regulate

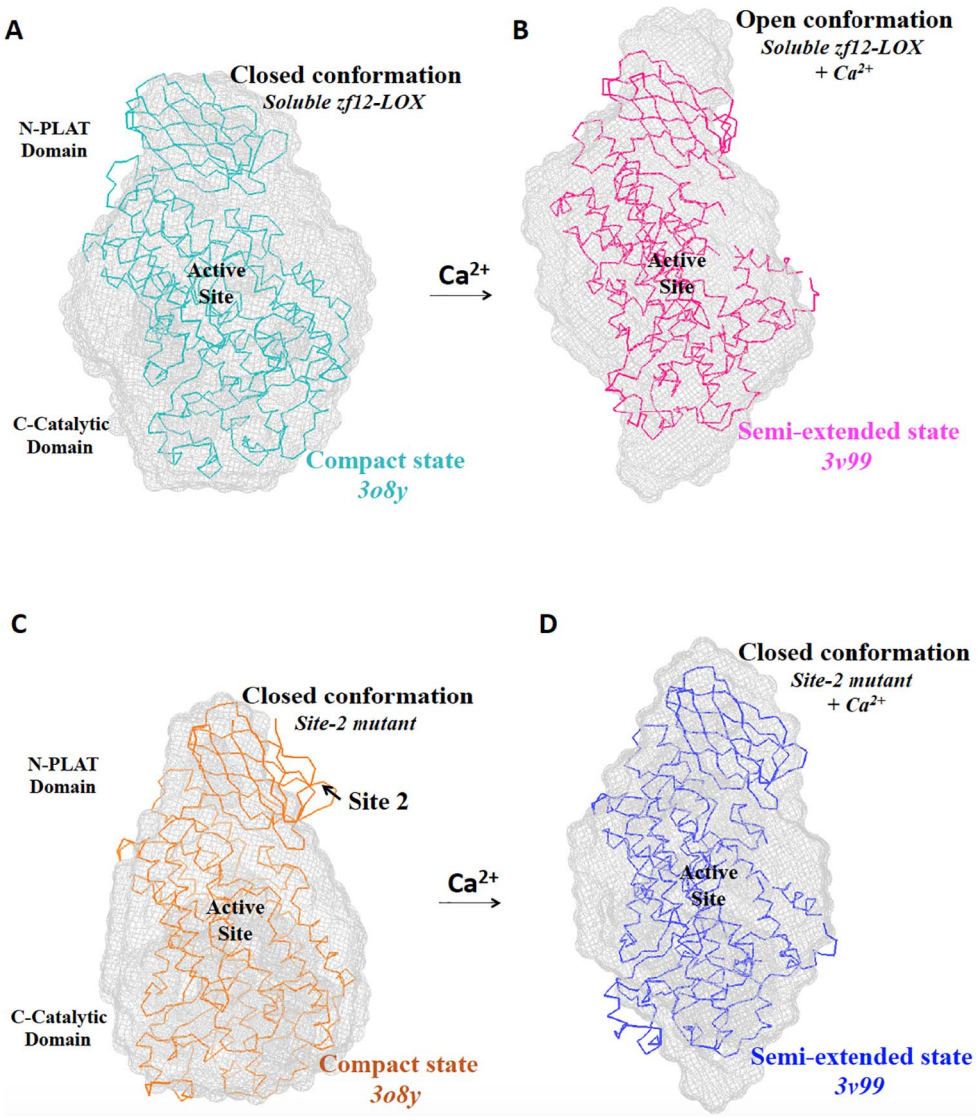

Fig. 8. Superimposition of SAXS solution structure (grey envelops) and crystal structure of h5-LOX (front view) for (A) soluble *zf*12-LOX, (B) soluble *zf*12-LOX + Ca^{2+}, (C) site-2 mutant and (D) site-2 mutant + Ca^{2+} respectively. The structural fitting highlights the 2-domain architecture of the *zf*12-LOX. Superimposition shows compact structure of h5-LOX (PDB 3o8y) matches to the closed conformation of *zf*12-LOX and site-2 mutant. However matching of semi-extended structure of soluble h5-LOX (PDB 3v99) with the calcium-bound states show an open-conformation for soluble *zf*12-LOX + Ca^{2+} and still closed-state for site-2 mutant + Ca^{2+}. All figures have been rendered by Pymol and similar color label represent the associated states.

enzyme activity. The calcium binding loops and the putative active site entrance 1 are on the same side of the molecule. Thus we speculate that Ca^{2+} binding and conformational distant movements of N-PLAT domain might facilitate substrate capture. An open-state of *zf*12-LOZ:Ca^{2+}, as seen in this study, provides an evidence for the above. This might encompass exposure of hydrophobic residues nearby as discussed earlier [9,58,61]. Thus it allows us to propose that *zf*12-LOX might switch from a closed (calcium-free) to open (calcium-bound) state(s) in solution as a mechanism of activation. The findings for *zf*12-LOX might hold true for mammalian LOXs and extend our understanding of the mechanism utilized for calcium regulation at molecular level.

Conflict of interest

The authors declare no conflicts of interest with the contents of this article.

Author's contribution

M. M. and M. H. share an equal authorship. M. M. and A. R. M. designed the work. M. M. performed experiments, analyzed data and prepared the manuscript. M. H. assisted in SAXS experiments and analysis. A. F. performed the MS experiments. N. B. helped in activity studies. M. H., C. W., O. R. and J. Z. H. contributed their advisory support during manuscript preparation. M. M. supervised the research. All authors reviewed the results and approved the final version of the manuscript.

Transparency document

The Transparency document associated with this article can be found, in the online version.

Acknowledgments

This work was supported by a grant from the Swedish Research Council (10350). We thank Michaela Mårback for technical assistance and the Protein Science Facility (PSF), Department of Medical Biochemistry and Biophysics, Karolinska Institute, Stockholm, Sweden for technical support. A.F. is funded by the Karin and Sten Mörtstedt initiative on Anaphylaxis. We also thank Prof. Jill Trewhella for valuable discussions regarding SAXS data processing and the staff at Petra III, P12 beamline, Hamburg and Max IV lab, Lund, for assistance in SAXS data collection.

Appendix A. Supplementary data

Supplementary data to this article can be found online at http://dx.doi.org/10.1016/j.bbagen.2017.05.015.

References

[1] K. Tang, K.V. Honn, 12(S)-HETE in cancer metastasis, Adv. Exp. Med. Biol. 447 (1999) 181–191.
[2] E.R. Greene, S. Huang, C.N. Serhan, D. Panigrahy, Regulation of inflammation in cancer by eicosanoids, Prostaglandins Other Lipid Mediat. 96 (2011) 27–36.
[3] M. Hersberger, Potential role of the lipoxygenase derived lipid mediators in atherosclerosis: leukotrienes, lipoxins and resolvins, Clin. Chem. Lab. Med. 48 (2010) 1063–1073.
[4] L.B. Fanning, J.A. Boyce, Lipid mediators and allergic diseases, Ann. Allergy Asthma Immunol. 111 (2013) 155–162.
[5] A.R. Brash, Lipoxygenases: occurrence, functions, catalysis, and acquisition of substrate, J. Biol. Chem. 274 (1999) 23679–23682.
[6] B. Samuelsson, S.E. Dahlen, J.E. Lindgren, C.A. Rouzer, C.N. Serhan, Leukotrienes and lipoxins: structures, biosynthesis and biological effects, Science 237 (1987) 1171–1176.
[7] S.A. Tatulian, J. Steczko, W. Minor, Uncovering a calcium-regulated membrane-binding mechanism for soybean lipoxygenase-1, Biochemistry 37 (1998) 15481–15490.
[8] I. Ivanov, H. Kuhn, D. Heydeck, Structural and functional biology of arachidonic acid 15-lipoxygenase-1 (ALOX15), Gene 573 (2015) 1–32.
[9] T. Hammarberg, O. Rådmark, 5-Lipoxygenase binds calcium, Biochemistry 38 (1999) 4441–4447.
[10] M.L. Oldham, A.R. Brash, M.E. Newcomer, Insights from the X-ray crystal structure of coral 8R-lipoxygenase: calcium activation via a C2-like domain and a structural basis of product chirality, J. Biol. Chem. 280 (2005) 39545–39552.
[11] A. Baba, S. Sakuma, H. Okamoto, T. Inoue, H. Iwata, Calcium induces membrane translocation of 12-lipoxygenase in rat platelets, J. Biol. Chem. 264 (1989) 15790–15795.
[12] R. Brinckmann, K. Schnurr, D. Heydeck, T. Rosenbach, G. Kolde, H. Kühn, Membrane translocation of 15-lipoxygenase in hematopoietic cells is calcium-dependent and activates the oxygenase activity of the enzyme, Blood 91 (1998) 64–74.
[13] M.J. Kobe, D.B. Neau, C.E. Mitchell, S.G. Bartlet, M.E. Newcomer, The structure of human 15-lipoxygenase-2 with a substrate mimic, J. Biol. Chem. 289 (2014) 8562–8569.
[14] R. Järving, A. Lokene, R. Kurg, L. Siimon, I. Järving, N. Samel, Activation of 11R-lipoxygenase is fully Ca^{2+}-dependent and controlled by the phospholipid composition of the target membrane, Biochemistry 51 (2012) 3310–3320.
[15] X.S. Chen, C.D. Funk, The N-terminal β-barrel domain of 5-lipoxygenase is essential for nuclear membrane translocation, J. Biol. Chem. 276 (2001) 811–818.
[16] T. Hammarberg, P. Provost, B. Persson, O. Rådmark, The N-terminal domain of 5-lipoxygenase binds calcium and mediates calcium stimulation of enzyme activity, J. Biol. Chem. 275 (2000) 38787–38793.
[17] S. Kulkarni, S. Das, C.D. Funk, D. Murray, W. Cho, Molecular basis of the specific subcellular localization of the C2-like domain of 5-lipoxygenase, J. Biol. Chem. 277 (2002) 13167–13174.
[18] O. Rådmark, O. Werz, D. Steinhilber, B. Samuelsson, 5-Lipoxygenase, a key enzyme for leukotriene biosynthesis in health and disease, Biochim. Biophys. Acta 4 (2015) 331–339.
[19] C.A. Rouzer, S. Kargman, Translocation of 5-lipoxygenase to the membrane in human leukocytes challenged with ionophore A23187, J. Biol. Chem. 263 (1988) 10980–10988.
[20] P. Borgeat, B. Samuelsson, Arachidonic acid metabolism in polymorphonuclear leukocytes: effects of ionophore A23187, Proc. Natl. Acad. Sci. U. S. A. 76 (5) (1979) 2148–2152.
[21] W. Shang, I. Ivanov, D. Svergun, O.Y. Borbulevych, A.M. Aleem, S. Stehling, J. Jankun, H. Kühn, E. Skrzypczak-Jankun, Probing dimerization and structural flexibility of mammalian lipoxygenases by small-angle X-ray scattering, J. Mol. Biol. 409 (2011) 654–668.
[22] M. Hammel, M. Walther, R. Prassl, H. Kuhn, Structural flexibility of the N-terminal beta-barrel domain of 15-lipoxygenase-1 probed by small angle X-ray scattering. Functional consequences for activity regulation and membrane binding, J. Mol. Biol. 343 (2009) 917–929.
[23] I. Ivanov, A. Di Venere, T. Horn, P. Scheerer, E. Nicolai, S. Stehling, C. Richter, E. Skrzypczak-Jankun, G. Mei, M. Maccarrone, H. Kühn, Tight association of N-terminal and catalytic subunits of rabbit 12/15-lipoxygenase is important for protein stability and catalytic activity, Biochim. Biophys. Acta 1811 (2011) 1001–1010.
[24] I. Ivanov, W. Shang, L. Toledo, L. Masgrau, D.I. Svergun, S. Stehling, H. Gómez, A. Di Venere, G. Mei, J.M. Lluch, Ligand-induced formation of transient dimers of mammalian 12/15-lipoxygenase: a key to allosteric behavior of this class of enzymes, Proteins 80 (2012) 703–712.
[25] E. Dainese, A. Sabatucci, G. van Zadelhoff, C.B. Angelucci, P. Vachette, G.A. Veldink, A.F. Agro, M. Maccarrone, Structural stability of soybean lipoxygenase-1 in solution as probed by small angle X-ray scattering, J. Mol. Biol. 349 (2005) 143–152.
[26] P. Eek, R. Järving, I. Järving, N.C. Gilbert, M.E. Newcomer, N. Samel, Structure of a calcium-dependent 11*R*-lipoxygenase suggests a mechanism for Ca^{2+} regulation, J. Biol. Chem. 287 (2012) 22377–22386.
[27] C.B. Klee, T.C. Vanaman, Calmodulin, Adv. Protein Chem. 35 (1982) 213–321.
[28] A. Geiger, L. Russo, T. Gensch, T. Thestrup, S. Becker, K.P. Hopfner, C. Griesinger, G. Witte, O. Griesbeck, Correlating calcium binding, Förster resonance energy transfer, and conformational change in the biosensor TN-XXL, Biophys. J. 102 (2012) 2401–2410.
[29] M. Michalak, J. Groenendyk, E. Szabo, L.I. Gold, M. Opas, Calreticulin, a multi-process calcium-buffering chaperone of the endoplasmic reticulum, Biochem. J. 417 (2009) 651–666.
[30] K.N. Toft, N. Larsen, F.S. Jorgensen, P. Hojrup, G. Houen, B. Vestergaard, Small angle X-ray scattering study of calreticulin reveals conformational plasticity, Biochim. Biophys. Acta 1784 (2008) 1265–1270.
[31] S.G. Boelt, C. Norn, M. Rasmussen, I. Andre, E. Ciplys, R. Slibinskas, G. Houen, P. Hojrup, Mapping the Ca^{2+} induced structural change in calreticulin, J. Proteome 142 (2016) 138–148.
[32] E. Bitto, C.A. Bingman, L. Bittova, R.O. Frederick, B.G. Fox, G.N. Phillips Jr., X-ray structure of *Danio rerio* secretagogin: a hexa-EF-hand calcium sensor, Proteins 76 (2009) 477–483.
[33] J. Chan, A.E. Whitten, C.M. Jeffries, I. Bosanac, T.K. Mal, J. Ito, H. Porumb, T. Michikawa, K. Mikoshiba, J. Trewhella, M. Ikura, Ligand-induced conformational changes via flexible linkers in the amino-terminal region of the inositol 1,4,5-trisphosphate receptor, J. Mol. Biol. 373 (2007) 1269–1280.
[34] D.J. Grunwald, J.S. Eisen, Headwaters of the zebrafish-emergence of a new model vertebrate, Nat. Rev. Genet. 3 (2002) 717–724.
[35] U. Haas, E. Raschperger, M. Hamberg, B. Samuelsson, K. Tryggvason, J.Z. Haeggström, Targeted knock-down of a structurally atypical zebrafish 12S-lipoxygenase leads to severe impairment of embryonic development, Proc. Natl. Acad. Sci. U. S. A. 108 (2011) 20479–20484.
[36] C.B. Kimmel, W.W. Ballard, S.R. Kimmel, B. Ullmann, T.F. Schilling, Stages of embryonic development of the zebrafish, Dev. Dyn. 203 (1995) 253–310.
[37] N.C. Gilbert, S.G. Barlett, M.T. Waight, D.B. Neau, W.E. Boeglin, A.R. Brash, M.E. Newcomer, The structure of human 5-lipoxygenase, Science 331 (2011) 217–219.
[38] M.J. Schilstra, G.A. Veldink, J. Verhagen, J.F.G. Vliegenthart, Effect of lipid hydroperoxide on lipoxygenase kinetics, Biochemistry 37 (1992) 7692–7699.
[39] M. Gibian, P. Vandenberg, Product yield in oxygenation of linoleate by soybean lipoxygenase: the value of the molar extinction coefficient in the spectrophotometric assay, Anal. Biochem. 163 (1987) 343–349.
[40] G. Senisterra, E. Markin, K. Yamazaki, R. Hui, US Patent Appl 20040072356, 2004.
[41] G. Senisterra, R. Hui, M. Vedadi, US Patent Appl 2005079526, 2005.
[42] G.A. Senisterra, E. Markin, K. Yamazaki, R. Hui, M. Vedadi, D.E. Awrey, Screening for ligands using a generic and high-throughput light-scattering-based assay, J. Biomol. Screen. 11 (2006) 940–948.
[43] A. Labrador, Y. Cerenius, C. Svensson, K. Theodor, T. Plivelic, The yellow mini-hutch for SAXS experiments at MAX IV Laboratory, J. Phys. Conf. Ser. 425 (2013) 1742–6596.
[44] P. Pernot, A. Round, R. Barrett, A.D.M. Antolinos, A. Gobbo, E. Gordon, S. McSweeney, Upgraded ESRF BM29 beamline for SAXS on macromolecules in solution, J. Synchrotron Radiat. 20 (2013).
[45] E. Gasteiger, C. Hoogland, A. Gattiker, S. Duvaud, M.R. Wilkins, R.D. Appel, A. Bairoch Protein Identification and Analysis Tools on the ExPASy Server, (2015).
[46] P.V. Konarev, V.V. Volkov, A.V. Sokolova, M.H.J. Koch, D.I. Svergun, PRIMUS - a Windows-PC based system for small-angle scattering data analysis, J. Appl. Crystallogr. 36 (2003) 1277–1282.
[47] D.I. Svergun, Determination of the regularization parameter in indirect-transform methods using perceptual criteria, J. Appl. Crystallogr. 25 (1992) 495–503.
[48] A. Guinier, La diffraction des rayons X aux trespetits angles; application a l'etude de phenomenes ultramicroscopiques, Ann. Phys. 12 (1939) 161–237.
[49] M.V. Petoukhov, D. Franke, A.V. Shkumatov, G. Tria, A.G. Kikhney, M. Gajda, C. Gorba, H.D. Mertens, P.V. Konarev, D.I. Svergun, J. Appl. Crystallogr. 45 (2012) 342–350.
[50] D.I. Svergun, M.V. Petoukhov, M.H.J. Koch, Determination of domain structure of proteins from X-ray solution scattering, Biophys. J. 80 (2001) 2946–2953.
[51] D.I. Svergun, Restoring low-resolution structure of biological macromolecules from solution scattering using simulated annealing, Biophys. J. (1999) 2879–2886.
[52] V.V. Volkov, D.I. Svergun, Uniqueness of ab-initio shape determination in small-angle scattering, J. Appl. Crystallogr. 36 (2003) 860–864.
[53] W.L. DeLano, The PyMOL Molecular Graphics System, DeLano Scientific, San Carlos, CA, USA, 2002 (http://www.pymol.org).
[54] M. Kozin, D. Svergun, Automated matching of high and low-resolution structural

models, J. Appl. Crystallogr. 34 (2001) 33–41.
[55] D.I. Svergun, C. Barberato, M.H.J. Koch, CRYSOL - a program to evaluate X-ray solution scattering of biological macromolecules from atomic coordinates, J. Appl. Crystallogr. 28 (1995) 768–773.
[56] T. Puustinen, M.M. Scheffer, B. Samuelsson, Regulation of the human leukocyte 5-lipoxygenase: stimulation by micromolar Ca^{2+} levels and phosphatidylcholine vesicles, Biochim. Biophys. Acta 960 (1988) 261–267.
[57] M.E. Newcomer, A.R. Brash, The structural basis for specificity in lipoxygenase catalysis, Protein Sci. 3 (2015) 298–309.
[58] I.A. Butovich, O.V. Kharchenko, Cooperativity in 5-lipoxygenase catalysis is caused by existence of an allosteric adsorption center at the enzyme surface and modulated by dodecylsulfate, Prostaglandins Leukot. Essent. Fat. Acids 57 (1997) 260.
[59] A.T. Wecksler, V. Kenyon, N.K. Garcia, J.D. Deschamps, W.A. van der Donk, T.R. Holman, Kinetic and structural investigations of the allosteric site in human epithelial 15-lipoxygenase-2, Biochemistry 48 (2009) 8721–8730.
[60] S. Moin, T. Hofer, R. Sattar, Z. Ul-Haq, Molecular dynamics simulation of mammalian 15S-lipoxygenase with AMBER force field, Eur. Biophys. J. 40 (2011) 715.
[61] M. Walther, R. Wiesner, H. Kühn, Investigations into calcium-dependent membrane association of 15-lipoxygenase-1. Mechanistic roles of surface-exposed hydrophobic amino acids and calcium, J. Biol. Chem. 279 (2004) 3717–3725.